Aerodynamic analysis of nonuniform trailing edge blowing

Dong Liang
Aero Engine (Group) Corporation of China, Beijing, China
Wenjie Wang
Beihang University, Beijing, China, and
Peter J. Thomas
University of Warwick, Coventry, UK

Abstract

Purpose – Numerical and experimental results for different oncoming base-flow conditions indicate that nonuniform trailing edge blowing (NTEB) can expand the performance range of compressors and reduce the thrust on the rotor, while the efficiency of the compressor can be improved by more than 2 per cent.

Design/methodology/approach – Relevant aerodynamic parameters, such as total pressure, ratio of efficiency and axial thrust, are calculated and analyzed under conditions with and without NTEB. Measurements are performed downstream of two adjacent stator blades, at seven equidistantly spaced reference locations. The experimental measurement of the interstage flow field used a dynamic four-hole probe with phase lock technique.

Findings – An axial low-speed single-stage compressor was established with flow field measurement system and nonuniform blowing system. NTEB was studied by means of numerical simulations and experiments, and it is found that the efficiency of the tested compressor can be improved by more than 2 per cent.

Originality/value – Unlike most of the previous research studies which mainly focused on the rotor/stator interaction and trailing edge uniform blowing, the research results summarized in the current paper on the stator/rotor interaction used inlet guide vanes for steady and unsteady calculations. An active control of the interstage flow field in a low-speed compressor was used to widen the working range and improve the performance of the compressor.

Keywords Aerodynamic improvement, Non-uniform trailing edge blowing, Stator/rotor interaction, Unsteady load

Paper type Research paper

Nomenclature

Symbols

v_t = turbulent viscosity (Pa·s);
χ = ratio between working variable and molecular viscosity;
$\tilde{\nu}$ = working variable (Pa·s);
ν = molecular viscosity (Pa·s);
$\overrightarrow{V}$ = velocity vector (m/s);
Q = source term (m/s^2);
d = distance to the closest wall (m);
S = magnitude of vorticity (1/s);
η_{s1} = efficiency of a compressor with TEB;
m = main flow rate (kg/s);
δ_m = blowing flow rate (kg/s);
T_1^* = inlet total temperature (K);
P_1^* = inlet total pressure (Pa);
$T_{3'}^*$ = outlet total temperature (K);
$P_{3'}^*$ = outlet total pressure (Pa);
T_ε^* = total temperature of the blowing flow (K);
P_ε^* = outlet total pressure of the blowing flow (Pa); and
$W_{cooling}$ = kinetic energy of the blowing flow (J).

Definitions, acronyms and abbreviations

TEB = trailing edge blowing;
NTEB = nonuniform trailing edge blowing;
IGV = inlet guide vane;
VSV = variable stator vane;
STEB = stator trailing edge blowing; and
RTEB = rotor trailing edge blowing.

Introduction

Axial compressors are one of the core components in aeroengines determining their aerodynamic performance. Modern aeroengines widely use inlet guide vanes (IGV) or

This paper is supported by the Aeronautical Science Foundation of China (No. 2015ZBN3008), the China Postdoctoral Science Foundation (No. 2016M591046) and the China Scholarship Council (No. 201809110025). The authors are very grateful to the reviewers and the editor for their constructive comments and valuable suggestions to improve the presentation of the paper.

Received 3 April 2018
Revised 10 May 2018
13 May 2018
Accepted 14 May 2018

The current issue and full text archive of this journal is available on Emerald Insight at: **www.emeraldinsight.com/1748-8842.htm**

Aircraft Engineering and Aerospace Technology
91/1 (2019) 134–144

[DOI 10.1108/AEAT-04-2018-0115]

variable stator vanes (VSV) to improve aerodynamic performance parameters such as overall flow, efficiency and pressure ratio. In practice, the trailing edge of an upstream stator or rotor blade will produce a wake, which will influence the aerodynamic performance of the downstream blade.

The flow becomes more complex downstream of the upstream trailing edge as illustrated in Sun and Zhou (1994). Vortex shedding from the trailing edge may, for instance, be induced. When vortices exist and propagate in the flow field, there will be a significant momentum loss and periodic stresses will act on the downstream blade. Obviously, this represents an adverse phenomenon for the impeller machinery flow. For example, both shock intensity and wake loss are discussed considering pulsating coolant ejection at various frequencies and blowing ratios. To this end, blunt and circular trailing edges, exposed to continuous blowing (at different rates), were compared by using steady simulations (Bernardini *et al.*, 2013).

The compressor interstage region is also one of the noise sources in the compressor. The interfacial area is the most important region for the compressor interstage region. A pulsating vane-trailing-edge-coolant was proposed to control the vane trailing edge shock interaction with the downstream rotor at the rotor passing frequency at different Mach numbers, ranging from subsonic to supersonic regimes at two engine representative Reynolds numbers (Saavedra *et al.*, 2017).

Losses because of mixing at inlet and outlet can be reduced effectively by decreasing the axial spacing and increasing the load on the blade (Smith, 1966; Adamczyk, 1996; Deregel and Tan, 1996). Interactions between the wake and the boundary layer were studied by means of adjusting the frequency and the intensity of the wake (Roberts and Denton, 1996; Hodson, 1985, 1998). The wake induction and control of the boundary-layer transition can be used to reduce the loss.

In an axial engine, extra air flow is commonly used for different purposes. Suction and pulsed-blowing flow results in a robust ability to delay separation (Wilson *et al.*, 2013). Tip blowing can control tip leakage in a high-pressure turbine cascade (Volino, 2017). However, blowing flow technology has been adopted mostly for turbine blade cooling (Khojasteh *et al.*, 2017).

Table I Parameters of the low-speed compressor

No. of stator	No. of rotor	Rotating speed (rpm)	Radius of casing (m)	Radius of hub (m)
6	11	3,000-8,000	0.201	0.110

Figure 1 Geometry of the stator/rotor and blowing holes

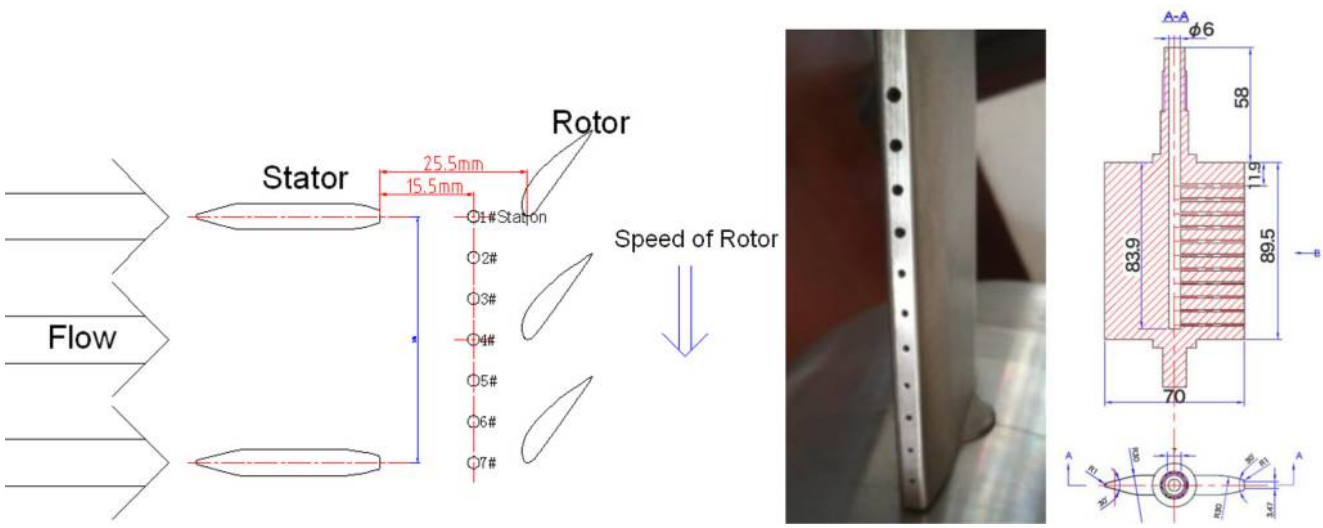

Figure 2 Compressor grid after approximation

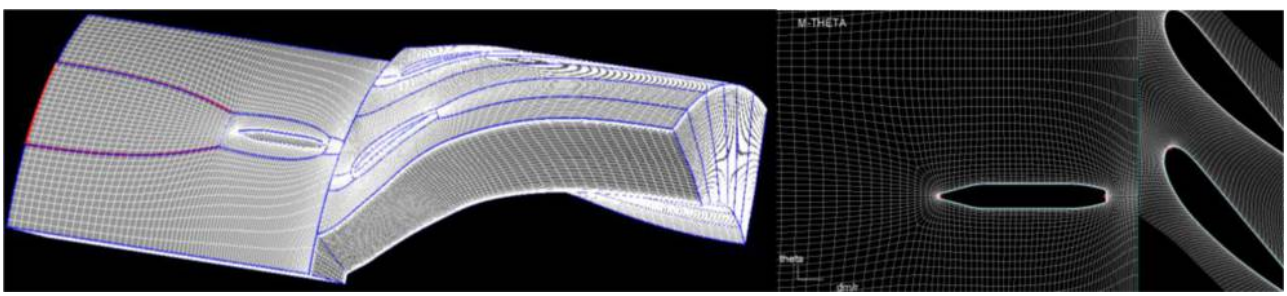

The method of trailing edge blowing (TEB) uses flow from the external or internal field being provided through the trailing edge of the blade to replenish the momentum loss in the wake region. As regard to the different types of blades, TEB distinguishes between the two categories of rotor trailing edge blowing (RTEB) and stator trailing edge blowing (STEB).

Figure 3 Distribution of y+ over stator and rotor

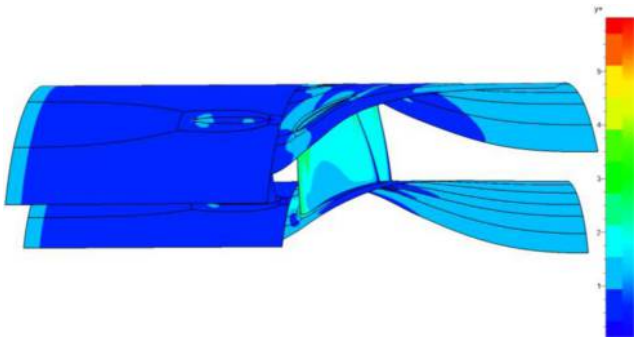

In 1996, Waitz studied boundary layer suction and RTEB as flow control methods to reduce rotor/stator interaction and unsteady load on the stator. The MISES, UNSFLO and LINSUB programs were used to calculate and simulate unsteady conditions. Waitz *et al.* (1996) and Sell (1996) investigated boundary layer suction and TEB with 2-D cascade experiments and concluded that TEB is a preferable method in comparison to boundary layer suction. Then, Brookfield (1998) and Brookfield and Waitz (2000) attempted to use TEB in a single-stage fan with 2 per cent of inlet flow. Their results showed that the relative Mach number distribution became well distributed.

Unlike the research on RTEB conducted at MIT, VA Tech studied STEB in a scaled transonic aeroengine with four stator blades and 1 per cent of inlet flow. Their results corroborated the conclusion of MIT in that TEB is the preferable method for reducing rotor/stator interaction and unsteady load on the blades (Saunders, 1998, 2000; Rao, 1999; Feng, 2000; Bailie, 2003; Craig, 2005; Halasz, 2005; Tweedie, 2006).

Therefore, most of the current research studies mainly focused on the rotor/stator interaction and uniform TEB. In the compressor, IGVs are different from stator blades because IGV

Figure 4 Grid independence analysis

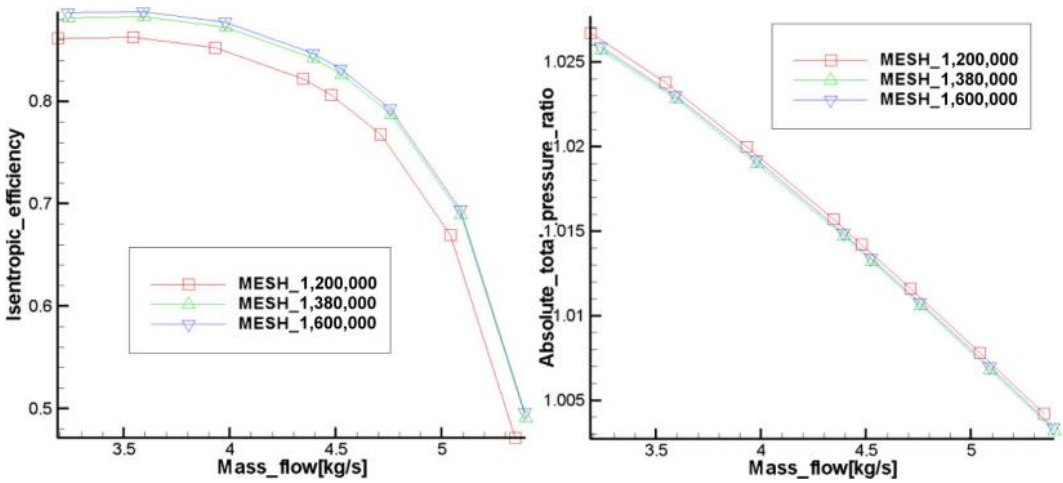

Figure 5 Characteristic lines with and without NTEB

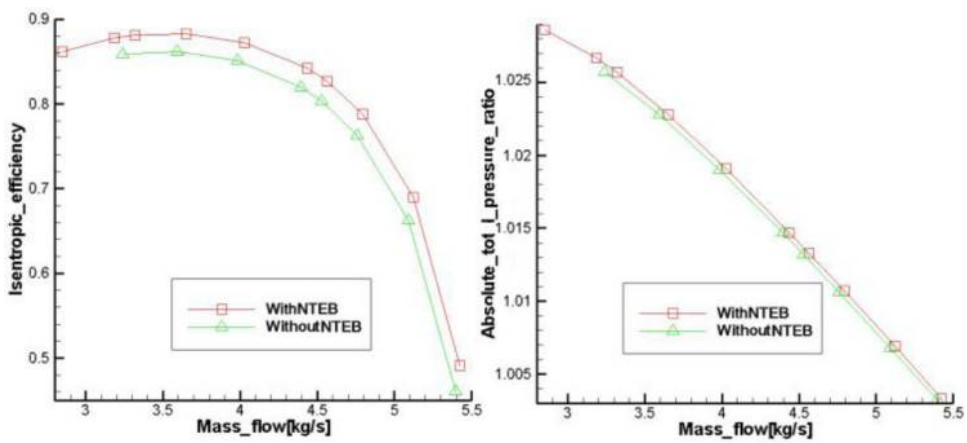

are usually much higher than rotor and stator. The research results summarized in the current paper on the stator/rotor interaction used IGVs for steady and unsteady calculations. An active control of the interstage flow field in a low-speed compressor was used to widen the working range and to improve the performance of the compressor. The numerical models and a low-speed compressor are described to reveal the characteristic parameters.

This paper mainly focuses on stator NTEB. The STEB method can make the flow more uniform. Thereby, it reduces the unsteady loads on the rotor blades, which are induced by the nonuniformity of the stator wake. This, in turn, reduces rotor fatigue and prolongs the service life of the rotor.

Numerical model

We have used the NUMECA software package for our numerical simulations. A central-difference scheme is used to discretize space, and a fourth-order Runge–Kutta method is used for the iterative time stepping. The turbulence model adopted is the Spalart–Allmaras model. This is a one-equation turbulence model which can be considered as a hybrid between the algebraic model of Baldwin–Lomax and two equation models. The main advantage of the Spalart–Allmaras model, in comparison to the Baldwin–Lomax model, is that the turbulent eddy viscosity field is always continuous. Its advantage over the k-ε model is mainly its robustness and the lower additional CPU and memory usage.

The turbulent viscosity v_t is given by:

$$\nu_t = \tilde{\nu} f_{\nu 1} \tag{1}$$

The function $f_{\nu 1}$ is defined by:

$$f_{\nu 1} = \frac{\chi^3}{\chi^3 + c_{\nu 1}} \tag{2}$$

where χ is the ratio between the working variable $\tilde{\nu}$ and the molecular viscosity v:

$$\chi = \frac{\tilde{\nu}}{\nu} \tag{3}$$

The turbulent working variable obeys the transport equation:

$$\frac{\partial \nu}{\partial t} + \vec{V} \cdot \nabla \tilde{v} = \frac{1}{\sigma}\{\nabla \cdot [(v + (1 + c_{b2})\tilde{v})\nabla \tilde{v}] - c_{b2}\tilde{v}\Delta\tilde{v}\} + Q \tag{4}$$

Table II Parameters with and without NTEB

	Flow (kg/s)	Total pressure ratio	Efficiency	Axial thrust (N)
Without NTEB	4.5278	1.0132	0.80349	−105.42
With NTEB	4.5643	1.0133	0.82641	−103.12

Table III Steady and unsteady aerodynamic parameters

	Flow (kg/s)	Total pressure ratio	Efficiency
Without NTEB			
Steady	4.5278	1.0132	0.80349
Unsteady time-average	4.5324	1.0131	0.82059
With NTEB			
Steady	4.5643	1.0133	0.82641
Unsteady time-average	4.5710	1.0132	0.84478

Figure 6 Velocity for different blade heights

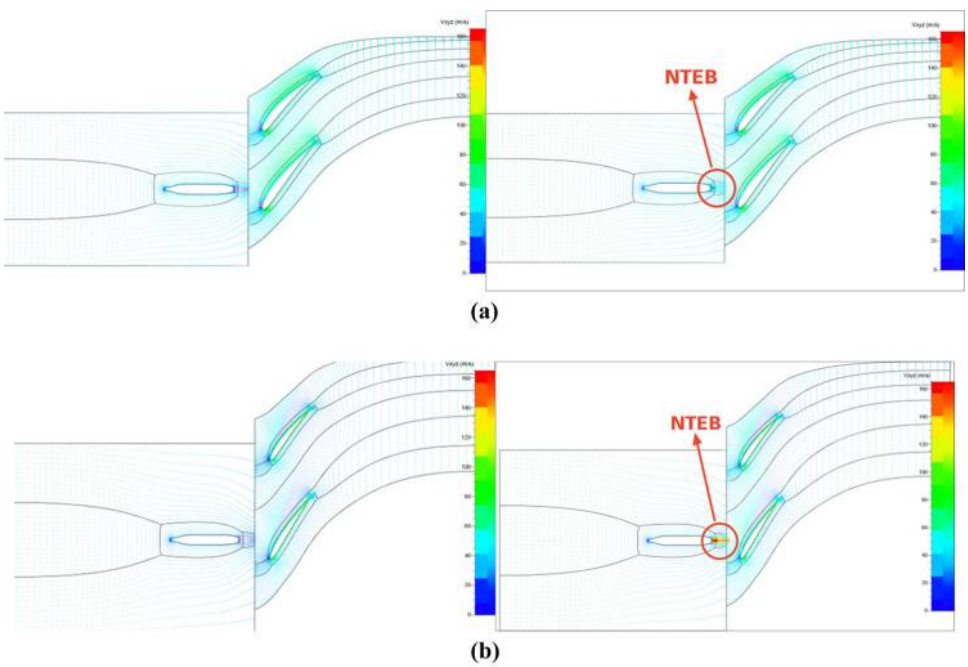

Notes: (a) S = 0.495; (b) S = 0.989

where $\vec{V}$ is the velocity vector, Q is the source term and σ, c_{b2} are constant.

The source term includes a production term and a destruction term:

$$Q = \tilde{\nu}P(\tilde{\nu}) - \tilde{\nu}D(\tilde{\nu}) \quad (5)$$

where

$$\tilde{\nu}P(\tilde{\nu}) = c_{b1}S\tilde{\nu} \quad (6)$$

$$\tilde{\nu}D(\tilde{\nu}) = c_{w1}f_w\left(\frac{\tilde{\nu}}{d}\right)^2 \quad (7)$$

$$\tilde{S} = Sf_{\nu 3} + \frac{\tilde{\nu}}{\kappa^2 d^2}f_{\nu 2} \quad (8)$$

Figure 7 Aerodynamic parameters as a function of time

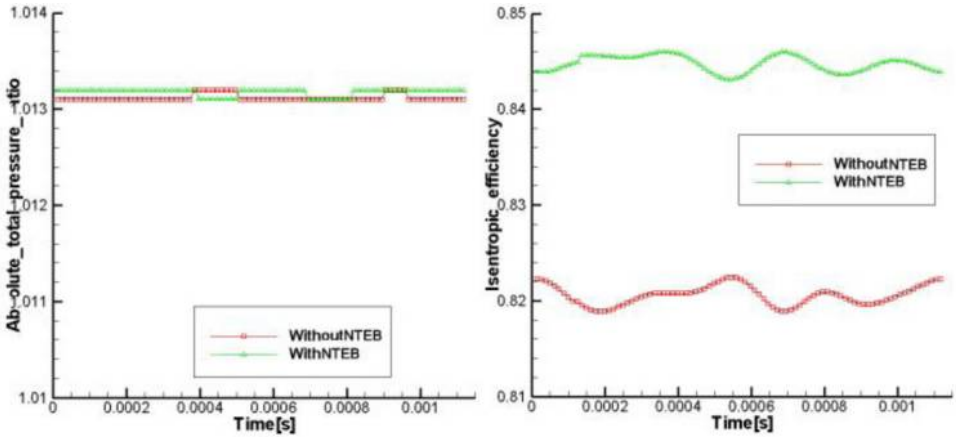

Figure 8 Total pressure without NTEB at S = 0.495

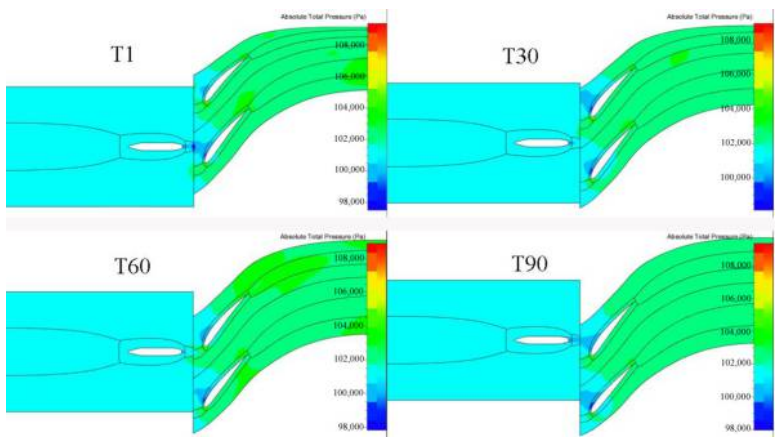

Figure 9 Total pressure without (Left 4) and with NTEB (Right 4) at S = 0.495

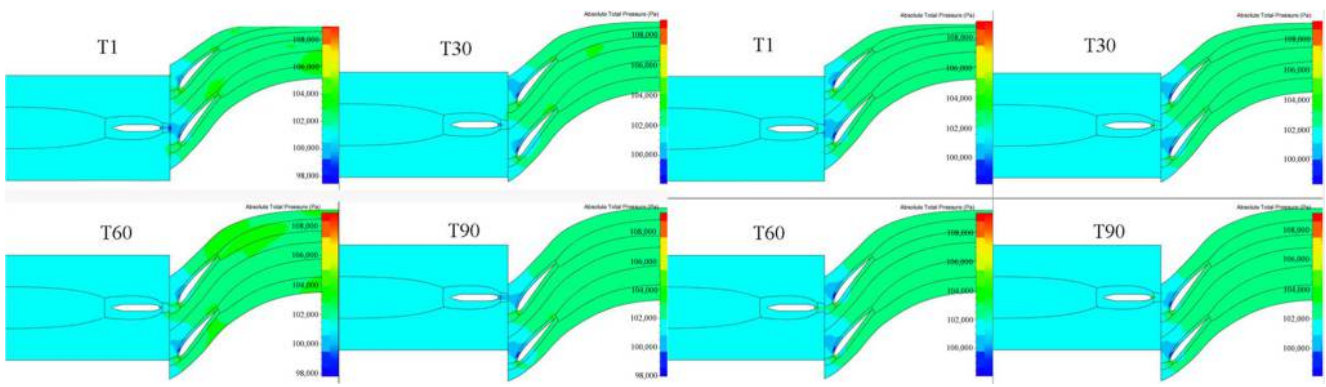

$$f_{v2} = \frac{1}{\left(1 + \chi/c_{v2}\right)^3} \tag{9}$$

$$f_{v3} = \frac{(1 + \chi f_{v1})(1 - f_{v2})}{\chi} \tag{10}$$

where d is the distance to the closest wall and S is the magnitude of vorticity.

In the destruction term [equation (7)], the function is as follows:

$$f_w = g\left(\frac{1 + c_{w3}^6}{g^6 + c_{w3}^6}\right)^{\frac{1}{6}} \tag{11}$$

with

$$g = r + c_{w2}(r^6 - r);\ r = \frac{\tilde{\nu}}{\tilde{S}\kappa^2 d^2} \tag{12}$$

The constants arising in the model are:

$$c_{w1} = c_{b1}/\kappa^2 + (1 + c_{b2})/\sigma, c_{w2} = 0.3, c_{w3} = 2, c_{v1} = 7.1,$$

$$c_{v2} = 5, c_{b1} = 0.1355, c_{b2} = 0.622, \kappa = 0.41, \sigma = 2/3 \tag{13}$$

Equation (4) is solved with appropriate boundary conditions: on a solid wall $\tilde{\nu} = 0$, along the inflow boundaries, the value is specified [v_t is obtained by using a Newton–Raphson procedure to solve equation (1)], and along the outflow boundaries, it is extrapolated from the interior values.

The principle of this turbulence model is based on the resolution of an additional transport equation for the eddy viscosity. The equation contains an advective, a diffusive and a source term and is implemented in a non-conservative manner. The cooling/bleed model allows both the simulation of cooling flows injected through walls into the flow or bleed flows where mass flow leaves the main flow through the wall. The adopted technique makes use of additional sources of mass, momentum and energy located at given points along given lines of the solid walls and does not require the grids of the cooling flow injection

Figure 10 Turbulent viscosity without (Left 4) and with NTEB (Right 4) at S = 0.495

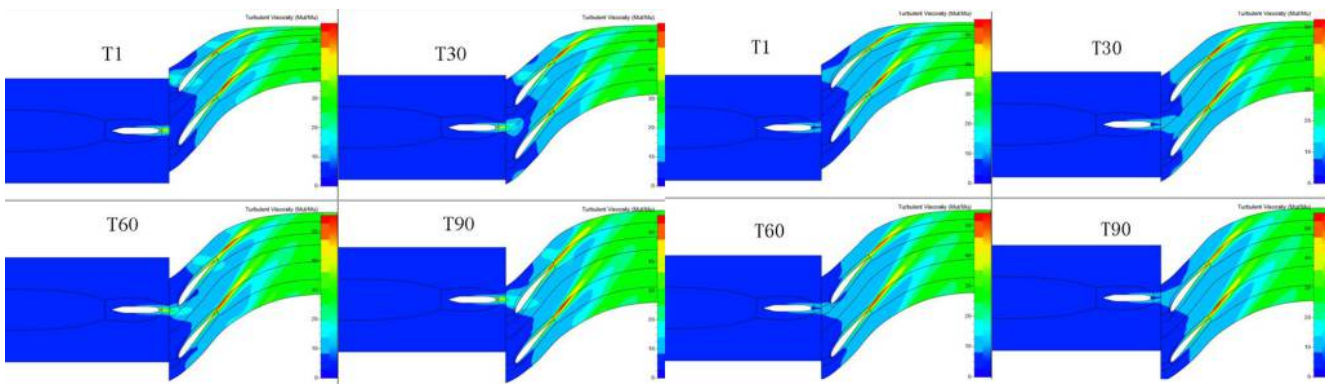

Figure 11 Total pressure and turbulent viscosity of observation point

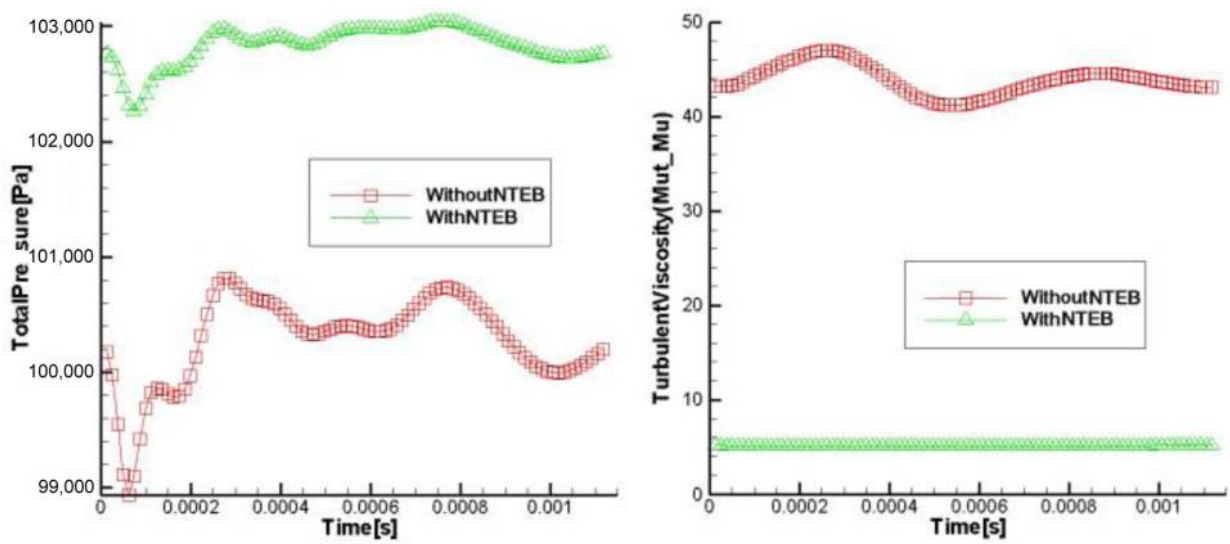

channels. The objective of this model is not to describe the details of the cooling flow itself but rather to consider its effect on the main flow. The efficiency of a compressor with TEB can be calculated by means of (Zhao, 2012):

$$\eta_{s1} = \frac{m \cdot C_p T_1^* \left[\left(\frac{P_{3'}^*}{P_1^*} \right)^{\frac{k-1}{k}} - 1 \right] + \delta m \cdot C_p \left(T_{3'}^* - T_\varepsilon^* \right)}{m \cdot C_p \left(T_{3'}^* - T_1^* \right) + \delta m \cdot C_p \left(T_{3'}^* - T_\varepsilon^* \right) + W_{cooling}} \quad (14)$$

where η_{s1} is the efficiency of a compressor with TEB, m is the main flow rate and δm is the blowing flow rate. T_1^* and P_1^* are the inlet total temperature and inlet total pressure, respectively. $T_{3'}^*$ and $P_{3'}^*$ are the outlet total temperature and outlet total pressure, respectively. T_ε^* and P_ε^* are the total temperature and outlet total pressure of the blowing flow. W_{cooling} is the kinetic energy of the blowing flow.

A multigrid method and local time step will result in accelerated convergence. The inlet boundary condition of the compressor in the numerical calculations used the parameters of the experimental condition for comparisons between the numerical results and the experimental results of the design points (Re = 699,301). That is, the inlet total pressure is 101,325 Pa, the inlet total temperature is 293 K, and the compressor outlet pressure is the average static pressure. During the simulation, the main working conditions of the compressor's characteristic curve are obtained by changing the outlet static pressure. In this process, the mixed plane method is adopted to ensure the conservation of flow, momentum and energy at the interface between stator and rotor.

Table IV Aerodynamic parameters with and without NTEB

Numerical conditions	Axial thrust (N)
Without NTEB	
Steady	−105.42
Unsteady time-average	−105.552
With NTEB	
Steady	−103.12
Unsteady time-average	−103.118

Figure 12 Axial thrust with time

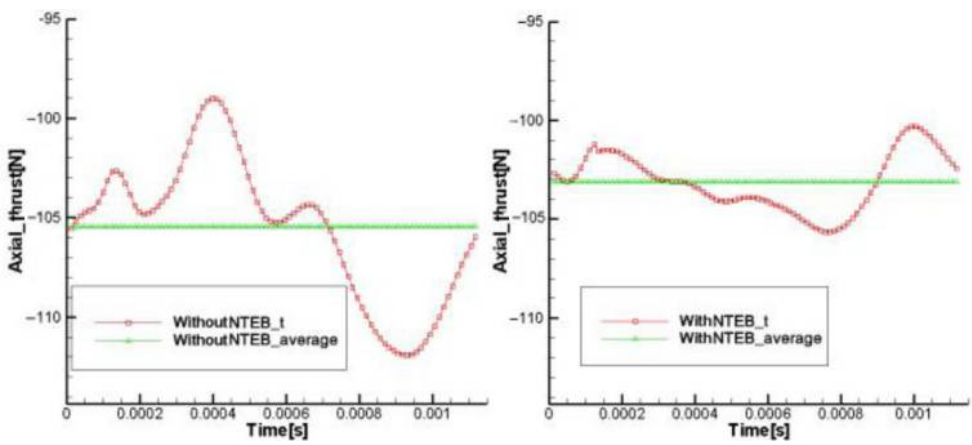

Low-speed compressor

A low-speed compressor, with an integrated TEB system was designed and built. Guide vanes in this compressor adopted VSV in a real engine. The technical specifications of the low-speed compressor are summarized in Table I.

Seven equidistantly spaced stations are distributed uniformly on the casing wall for flow-field measurement between the stator and the rotor as illustrated in Figure 1. The TEB system was connected to a high-pressure tank. The pressure of the flow from this tank can reach values as high as 0.8 MPa. The volume flow from a single blade can be 6.0 m^3/h, which is about 5 ‰ of inlet total flow.

Grid analysis

To facilitate steady and unsteady calculations and avoid full-size calculation, the ratio of stator and rotor is 1:2 after approximation. Therefore, one flow path contained one VSV and two rotor blades, in Figure 2; structured grids used HOH type and O type of grid around the blade after the near-wall grid is densified. The tip clearance is 0.91 mm which is about 1 per cent of the blade height.

At least three-nested grids ensure the grid quality. There are no negative cells, and the orthogonality is bigger than 15°. The aspect ratio is less than 2,000, and the expansion ratio is less than 3. The most important part of the grids for NTEB calculations is the grid between stator and rotor as shown in Figure 2.

Figure 13 Four-hole dynamic pressure probe

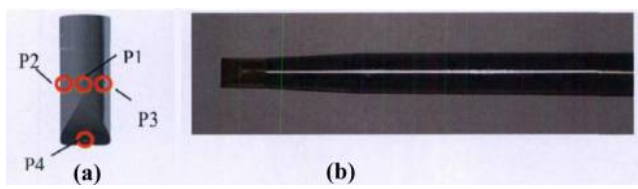

In Figure 3, the distribution of y+ over stator and rotor is illustrated to show the quantitative data. The values of y+ centered on less than 3 can satisfy the requirement of the numerical model (y+<10). To analyze the grid independence, three different numbers of grid points are used for the calculation of the characteristic line as shown in Figure 4. Finally, the optimum number of grid points for the balance between accuracy and time required to finish calculation is 1.38 million.

Steady numerical simulation

In the numerical calculations, the blowing holes are integrated in the stator trailing edge, which corresponds to the arrangement of the experimental stator blade. The six blowing holes are located along the radial direction of the stator blade, which correspond to the locations of blade height (S = 0.989, 0.824, 0.659, 0.495, 0.330 and 0.165). The oncoming mass flow rate in simulation and experiment is 0.1 kg/s corresponding to approximately 2.2 per cent of the inlet flow. The gas parameters of the NTEB boundary condition are the same as the parameters of the inlet boundary condition.

Figure 5 reveals that NTEB shifts the efficiency curve and pressure ratio curve to higher values. However, the flow blockage point was basically unchanged. Nevertheless, the surge point was significantly shifted. This indicated that NTEB can expand the working range of the compressor.

The summary of the relevant performance parameters, in Table II, at the points show that NTEB has increased the efficiency of the compressor.Figure 6 reveals that NTEB improves the stator wake. It can be seen that NTEB reduces the number of vortices, enlarges the stall margin and replenishes the total pressure loss in the wake region.

Figure 14 P1 at different stations

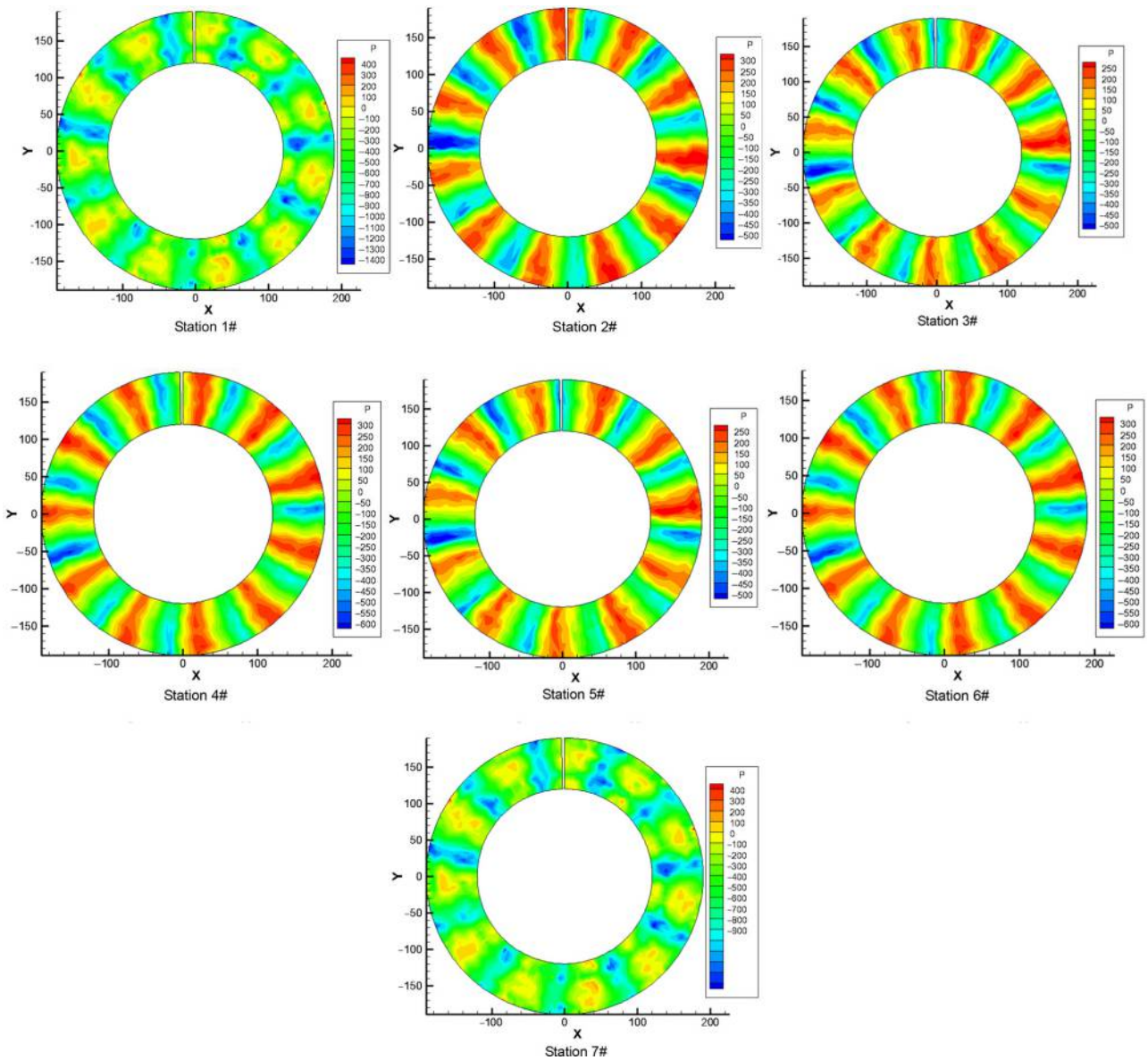

Unsteady numerical calculation

All aerodynamic parameters for the unsteady time-average are similar to those of the steady calculation except for the efficiency in Table III, and the results of the steady calculation provide the initial conditions/fields for the unsteady calculations. This ensures that the results for the unsteady calculations are reliable. The efficiency of the unsteady time-average is expected to be different from that of the steady condition because the working conditions are very different.

Analysis of the turbulent viscosity and the total pressure

The aerodynamic parameters of this low-speed compressor with and without TEB changed with time as shown in Figure 7. It is evident that the total pressure ratio with TEB is almost unchanged from the case where TEB is absent, whereas TEB improves the efficiency.

The total pressure in the flow field with NTEB is compared with the field without TEB at the blade height (S = 0.495). The flow fields without NTEB, at four time, are shown in Figure 8.

The total pressure, without NTEB and at four different times are displayed in Figure 8. There exists a relatively wide wake region downstream of the trailing edge of the stator. In this wake region, vortices are evident, and the turbulent viscosity and the total pressure loss are much more pronounced. The wake is seen to move downstream with time. The stator/rotor interaction occurred when the wake from the trailing edge of the stator acted on the downstream rotor. This will undoubtedly influence aerodynamic performance of the downstream rotor.

The turbulent viscosity and total pressure for the unsteady calculations with NTEB are shown in Figures 9 and 10. The vortex dissipation in the wake region is recovered with blowing flows. The total pressure loss and turbulent viscosity are reduced.

The observation point (0.0, 0.155, 0.04) located in the wake region which is 0.005 m away from stator trailing edge at the blade height S = 0.495. The total pressure and turbulent viscosity of the observation point with time are shown in Figure 11, which indicates that NTEB can reduce the turbulent viscosity.

In Figure 11, the total pressure loss and the turbulent viscosity are necessarily high because the observation point is in the wake region. The vortex at the observation point is essentially eliminated, the total pressure loss is reduced and turbulent viscosity is reduced with NTEB.

Analysis of the axial thrust

The axial thrust of the steady results is almost the same as the unsteady time-averaged results in Table IV. This indicates that the numerical calculations are reliable. But the axial thrust of the downstream rotor with NTEB is 2.3 N lower than without NTEB.

The axial thrusts of steady and unsteady time-average are shown in Figure 12. The axial thrust in the flow path fluctuated around the time-average value. The maximum amplitude

Figure 15 P1 of different blowing flows

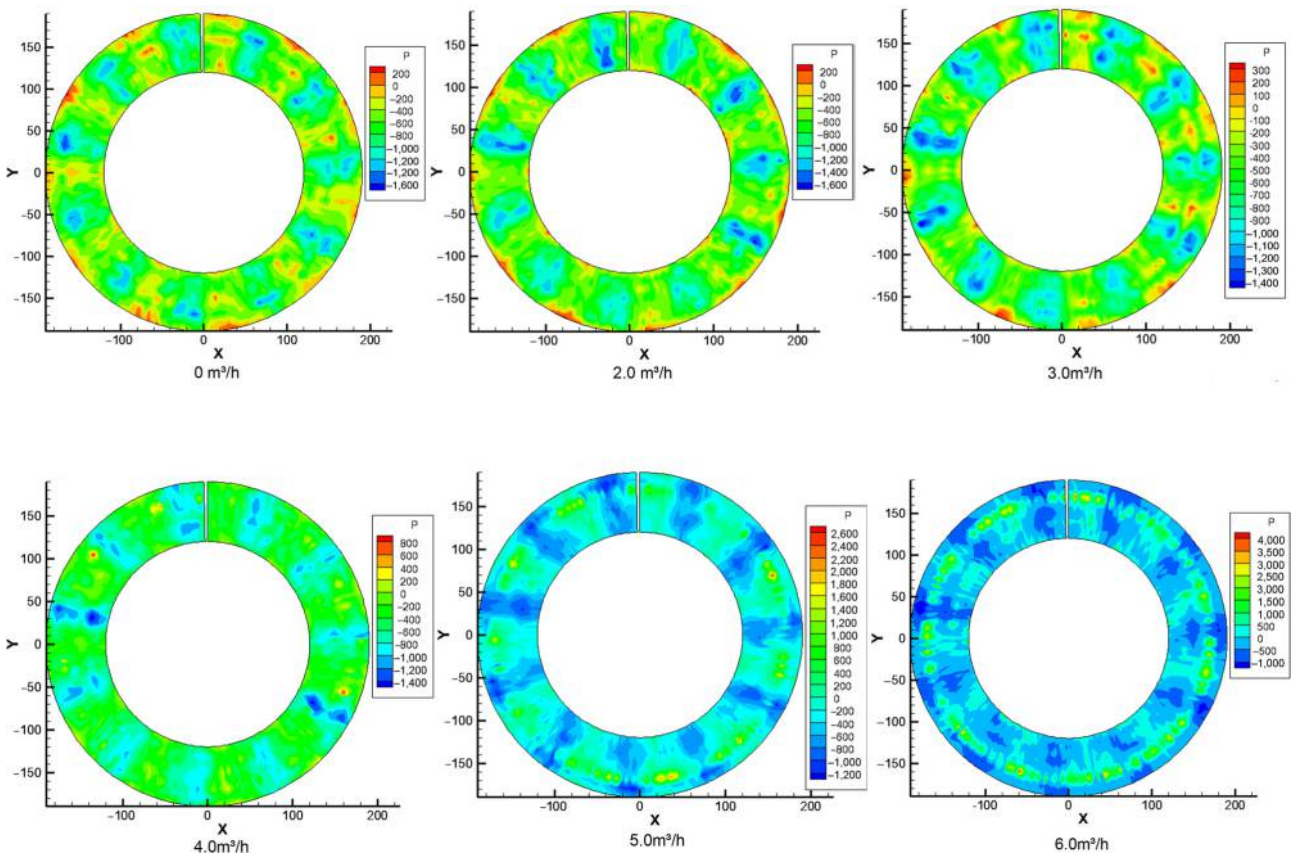

fluctuation without and with NTEB/TEB is about 6.56 and 2.52 N, respectively. The axial thrust on the downstream rotor and vibration amplitude are reduced.

Flow field measurement for the low-speed compressor

A dynamic four-hole pressure probe is adopted to measure the flow field. We choose *P1* of the probe as the parameter in Figure 13. Some flow measurement results are discussed to illustrate the stator wake region.

The gap in every flow field measurement result of Figures 14 and 15 indicates the location of the four-hole probe. With the exception of the measurement results at Locations 1 and 7, the flow field at the other stations are periodic because of these two stations being away from the unsteady flow from upstream stator blade during rotor rotating. The periodicity in Figure 14 is equal to the number of rotor blades because the stator/rotor interaction is excited by the downstream rotor.

It can be seen from the measurement results that *P1* is negative at Locations 1 and 7 because of the unsteady flow. The values at Locations 1 and 7 are far less than pressures at other stations. This means that the axial velocity loss is bigger in this area. The measurement results of *P1* at Location 1 for different NTEB situations are shown in Figure 15.

Negative values of *P1* at Station 1 are much bigger without NTEB because this position is immediately downstream of the stator. After blowing flow is added in the wake region, the magnitude of *P1* increased and the influence region widened. That illustrated that NTEB can improve the wake region.

Conclusion

This paper has focused on the stator/rotor interaction of stator blades with blowing holes. In the numeral calculations, the efficiency curve and pressure ratio curve moved up when TEB was applied, in comparison to the case where TEB is absent. Meanwhile, flow at the plugged point was basically unchanged. But the surge point was significantly shifted. This indicated that TEB can expand the working range of the compressor, while the thrust of rotor is reduced. TEB can obviously improve the stator wake, reduce wake vortex and recover the total pressure loss in the wake region. The total pressure ratio with TEB is almost unchanged from that without TEB. However, the efficiency when TEB was applied is improved in comparison to the case when TEB is absent. The experimental results also indicate that TEB can improve and even the flow field, reduce the thrust on the rotor and expand the working range of the compressor.

References

Adamczyk, J.J. (1996), "Wake mixing in axial flow compressors", *ASME*.

Bailie, S.T. (2003), *Effect of Inlet Guide Vane Flow Control on Forced Response of a Transonic Fan*, VT Polytechnic and State University, Blacksburg, VA.

Bernardini, C., Simone, S., Francesco, M., Guillermo, P. and Bayindir, H.S. (2013), "Pulsating coolant ejection effects downstream of supersonic trailing edge", *Engineering Applications of Computational Fluid Mechanics*, Vol. 7 No. 2, pp. 250-260.

Brookfield, J.M. (1998), *Turbofan Rotor/Stator Interaction Noise Reduction through Trailing Edge Blowing*, MIT.

Brookfield, J.M. and Waitz, I. (2000), "A trailing-edge blowing for reduction of turbomachinery fan noise", *Journal of Propulsion and Power*, Vol. 16 No. 1, pp. 57-64.

Craig, M.E. (2005), "Trailing edge blowing of model fan blades for wake management", MS thesis, Virginia Polytechnic and State University, Blacksburg, VA.

Deregel, P. and Tan, C.S. (1996), "Impact of rotor wakes on steady state axial compressor performance", *ASME*.

Feng, J.W. (2000), *Active Control for Reduction of Unsteady Stator-Rotor Interaction in a Turbofan Simulator*, VT Polytechnic and State University, Blacksburg, VA.

Halasz, C.W. (2005), *Advanced Trailing Edge Blowing Concepts for Fan Noise Control Experimental Validation*, VT Polytechnic and State University, Blacksburg, VA.

Hodson, H.P. (1985), "Measurements of wake-generated unsteadiness in the rotor passages of axial flow turbines", *ASME Journal of Engineering of Gas, Turbines and Power*, Vol. 107, pp. 467-476.

Hodson, H.P. (1998), "Blade row interference effects in axial turbomachinery stages", *VKI Lecture Series*, Vol. 1998 No. 2.

Khojasteh, A.R., Wang, S.F. and Peng, D. (2017), "Structure analysis of adiabatic film cooling effectiveness in the near field of a single inclined jet: measurement using fast-response pressure-sensitive paint", *International Journal of Heat and Mass Transfer*, Vol. 110, pp. 629-642.

Rao, N.M. (1999), *Reduction of Unsteady Stator-Rotor Interaction by Trailing Edge Blowing Using MEMS Based Microvalves*, VT Polytechnic and State University, Blacksburg, VA.

Roberts, Q.D. and Denton, J.D. (1996), "Loss production in the wake of a simulated subsonic turbine blade", *ASME*.

Saavedra, J., Paniagua, G. and Saracoglu, B.H. (2017), "Experimental characterization of the vane heat flux under pulsating trailing-edge blowing", *Journal of Turbomachinery*, Vol. 139 No. 6, -061004. p.

Saunders, C.A. (1998), *Noise Reduction in an Axisymmetric Supersonic Inlet Using Trailing Edge Blowing*, VT Polytechnic and State University, Blacksburg, VA.

Sell, J. (1996), *Cascade Testing to Assess the Effectiveness of Mass Addition/Removal Wake Management Strategies for Reduction of Rotor-Stator Interaction Noise*, MIT.

Smith, L.H. (1966), "Wake dispersion in turbomachines", *Journal of Basic Engineering, ASME Transactions*, Vol. 88 No. 3, pp. 689-690.

Sun, X. and Zhou, S. (1994), *Aeroacoustics*, National Defense Industry Press, pp. 75-90.

Tweedie, S. (2006), *Experimental Investigation of Flow Control Techniques to Reduce Hydroacoustic Rotor-Stator Interaction Noise*, VT Polytechnic and State University, Blacksburg, VA.

Volino, R.J. (2017), "Control of tip leakage in a high-pressure turbine Cascade using tip blowing", *Journal of Turbomachinery*, Vol. 139 No. 6, p. 061008.

Waitz, I.A., Brookfield, J.M., Sell, J. and Hayden, B.J. (1996), "Preliminary assessment of wake management strategies for

reduction of turbomachinery fan noise", *Journal of Propulsion and Power*, Vol. 12 No. 5, pp. 958-966.

Wilson, J., Schatzman, D. and Arad, E. (2013), "Suction and pulsed-blowing flow control applied to an axisymmetric body", *AIAA Journal*, Vol. 51 No. 10, pp. 2432-2446.

Zhao, B. (2012), *Applied Exploration and Mechanism Research on Enhancing the Compressor Performance by Air System Bleeding*, Beihang University, Beijing, pp. 52-56.

Further reading

Leitch, T.A., Saunders, C.A. and Ng, W.F. (2000), "Reduction of unsteady stator rotor interaction using trailing edge blowing", *Journal of Sound and Vibration*, Vol. 235 No. 2, pp. 235-245.

Corresponding author

Wenjie Wang can be contacted at: wangwenjie@buaa.edu.cn